Journal of The Electrochemical Society

The Electrochemical Reaction Mechanism of Tin Phosphide with Sodium

The Electrochemical Reaction Mechanism of Tin Phosphide with Sodium

Lituo Zheng,[a,*] R. A. Dunlap,[b,c,d] and M. N. Obrovac[a,b,c,,z]**

[a]*Department of Chemistry, Dalhousie University, Halifax, Nova Scotia B3H 4R2, Canada*
[b]*Department of Physics and Atmospheric Science, Dalhousie University, Halifax, Nova Scotia B3H 4R2, Canada*
[c]*Institute for Research in Materials, Dalhousie University, Halifax, Nova Scotia B3H 4R2, Canada*
[d]*College of Sustainability, Dalhousie University, Halifax, Nova Scotia B3H 4R2, Canada*

The sodiation mechanism of Sn_4P_3 was studied by ex-situ X-ray diffraction and Mössbauer effect spectroscopy. These results show that Sn_4P_3 is initially amorphized during sodiation, and suggest that upon further sodiation both Sn and P react simultaneously with Na to form Na_3P, $Na_{0.6}Sn$, and Na_4Sn_4. Upon further sodiation, the Na-Sn phases react with Na to make Na_5Sn_2 and $Na_{15}Sn_4$. These results are consistent with the behavior of Sn_4P_3 in Li cells.

Manuscript submitted October 21, 2015; revised manuscript received March 28, 2016. Published April 8, 2016.

Sodium ion batteries are considered to be one alternative to the currently widely-used lithium ion batteries.[1] However, the lack of appropriate anode materials hinders their development. Like lithium ion batteries, the use of a sodium metal as anode material in sodium ion batteries suffers from poor coulombic efficiency and a severe dendrite problem that can cause safety concerns.[2] Therefore, developing appropriate anode materials is of great importance in the progress of advancing sodium ion batteries.

Alloy materials have high energy density and have been proposed to for use as anode materials for sodium ion batteries.[3] Sn_4P_3 is a promising anode material for sodium ion batteries. It has a theoretical capacity of 1132 mAh/g or 1292 Ah/L, assuming the fully sodiated product is $Na_{15}Sn_4$ and Na_3P. Here, to be reflect their performance in full cells, the volumetric capacity is calculated at full volume expansion.[4] Recently, Qian et al.[5] and Kim et al.[6] reported that using Sn_4P_3 provides impressive cycle life in Na batteries (>100 cycles) as well as good reversible capacity (>600 mAh/g or 700 Ah/L).

This study aims to provide a deeper understanding of the sodiation mechanism of Sn_4P_3 using ex-situ X-ray diffraction (XRD) and Mössbauer spectroscopy. Room temperature ^{119}Sn Mössbauer spectroscopy has been successfully used to help understand the lithiation or sodiation mechanism of Sn or Sn-containing compounds.[7,8] Pérez-Vicente used ^{119}Sn Mössbauer spectroscopy to explain the lithiation process of Sn_4P_3.[9] Baggetto et al.[10] and Du et al.[11] used ^{119}Sn Mössbauer spectroscopy to determine the sodiation extent of Sn. Knowledge from these studies are important to shed light on the sodiation mechanism of Sn alloys. Here the utility of Mössbauer spectroscopy for the investigation of the sodiation mechanism of Sn_4P_3 is demonstrated.

Experimental

Sn_4P_3 was synthesized via high-energy ball milling. Stoichiometric amounts of Sn (-325 mesh, Alfa Aesar, 99.8%) and red phosphorus (Anachemia) powders were loaded under an argon atmosphere into 65 mL hardened steel ball-mill vials with 0.5 in. hardened steel balls at a ball-to-powder mass ratio of 20:1 (typically 2 grams of sample and 40 grams of balls). Ball milling was conducted with SPEX mill (Model 8000-D, Spex Certiprip, Metuchen, N.J.) for 1 hour. Samples were then immediately transferred to an argon-filled glove box without air exposure.

All electrode preparation was performed in an argon-filled glove box. Electrodes used for electrochemical measurements and ex-situ X-ray diffraction measurements consisted of a mixture of 80% by weight Sn_4P_3 powder, 10% carbon black (Super P, Erachem Europe), and 10% polyimide (PI-2555, HD Microsystems, 20% in N-methyl-2-pyrrolidone). These components were mixed in N-methyl-2-pyrrolidone (Sigma Aldrich, anhydrous 99.5%) with two tungsten carbide balls in a Retsch PM200 rotary mill (100 rpm, 1 hour) to create a uniform slurry. The slurry was then spread onto aluminum foil with a coating bar having a 0.004 in. gap (cells for Mössbauer studies were made from coating bar with a 0.012 in. gap) and dried under vacuum at 120°C overnight. 1.3 cm^2 circular electrodes were punched from the resulting coatings and heated at 300°C for 3 hours in flowing Ar before being taken into a glove box.

Electrodes were assembled in 2325-type coin cells. Na disks punched from thin foil (~0.015 inch) rolled from sodium ingot (Sigma Aldrich, ACS reagent grade) were used as counter/reference electrodes. Two Celgard 2300 and one blown microfiber separator (3M Company) were used as separators. 1 M $NaPF_6$ (Aldrich, 98%) in a solution of ethylene carbonate, diethyl carbonate and monofluoroethylene carbonate (volume ratio 3:6:1, from BASF) was used as electrolyte. Cells were cycled between 0.005 V and 1.5 V with a Maccor Series 4000 Automated Test System at a C/20 rate and trickled discharged to C/50 rate. Cells for Mössbauer studies were cycled at C/100 rate.

Cells for ex-situ XRD and Mössbauer studies were opened at different cutoff voltages in an Ar-filled glove box, using a special cell opener (DPM Solutions, Hebbville NS) to avoid short circuiting the electrode. For XRD studies, electrodes were first carefully removed from their current collector and then rinsed with dimethyl carbonate (DMC, BASF) several times to remove any residual salt. Samples were then sealed in an air-tight X-ray sample holder described by Fielden et al.[12] (DPM Solutions, Hebbville NS) in an Ar-filled glove box. X-ray diffraction patterns were collected using a JD2000 diffractometer equipped with a Cu Kα X-ray source (Kα = 1.54 Å) and a diffracted beam monochromator.

Several electrodes opened at the same cutoff voltage were stacked together into a circular plastic Mössbauer holder in order to gain sufficient mass for Mössbauer effect spectra. The holders were heat sealed in metallized plastic pouches in an Ar-filled glove box. Room temperature ^{119}Sn Mössbauer effect spectra were recorded in a constant-acceleration Wissel System II spectrometer equipped with a $CaSnO_3$ source. The spectrometer was calibrated using a composite absorber made of $BaSnO_3$ (room temperature center shift 0 mm/s) and metallic Sn (room temperature center shift +2.56 mm/s).

*Electrochemical Society Student Member.
**Electrochemical Society Member.
[z]E-mail: mnobrovac@dal.ca

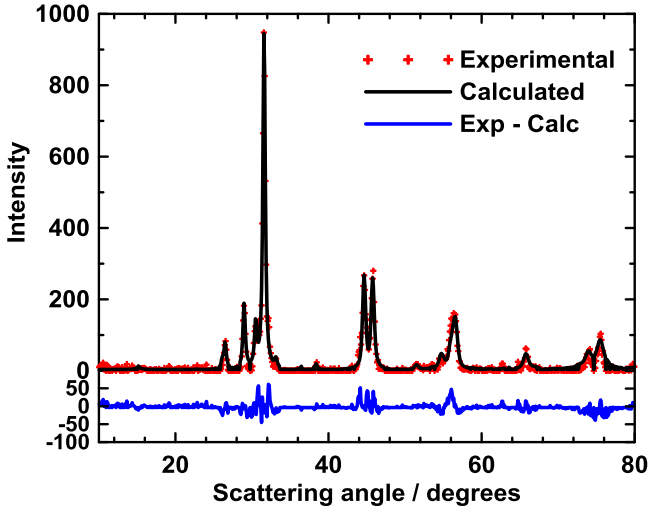

Figure 1. X-ray diffraction pattern and the Rietveld refinement.

Results and Discussion

Figure 1 shows the X-ray diffraction (XRD) pattern and the Rietveld refinement of synthesized Sn_4P_3. The XRD pattern comprises sharp peaks characteristic of crystalline phases. All the peaks and measured lattice constants (a = b = 3.976 Å, c = 35.3293 Å, $\alpha = \beta = 90^\circ$, $\gamma = 120^\circ$) are in good agreement with literature data for Sn_4P_3 (JCPDS No. 20-1294). Figure 2a shows the voltage curve of the first few cycles of a Sn_4P_3 vs Na coin cell and its differential capacity (dQ/dV) curve for the first two cycles is shown in Figure 2b. The capacity of the first discharge is similar to previously reported value (>1000 mAh/g); however, the cell shows a higher reversible capacity of more than 900 mAh/g, in comparison with about 700 mAh/g previously reported by Qian et al. and Kim et al.[5,6] This may be attributed to the better binding effect of polyimide with alloy materials and to its electrochemical activity,[13] as Qian et al. and Kim et al. used inactive CMC and PAA as their binders, respectively.[5,6]

The discharge curve has three main features: a steep sloping plateau with a capacity of 100 mAh/g, followed by a less steep voltage plateau at about 0.3 V with a capacity of about 700 mAh/g, and finally a nearly flat plateau at very low voltage (close to 0.005V) with a capacity of 1100 mAh/g. The voltage profile during charge is also composed of three main plateaus. These plateaus can also be observed as three main peaks in the differential capacity during both discharge and charge. The hysteresis during cycling is about 0.3 V.

According to previous studies of the sodiation of Sn, the $Na_{0.6}Sn$ phase forms at about 0.4 V vs. Na^+/Na,[10] Na_4Sn_4 forms at about 0.2 V vs. Na^+/Na,[11] Na_5Sn_2 forms at about 0.1 V vs. Na^+/Na and $Na_{15}Sn_4$ forms at a voltage near 0 V.[11] This data can be used to predict which Sn-Na phases could be present at different cutoff voltages in the sodiation process of Sn_4P_3. Figure 3a shows the ex-situ XRD patterns of tin phosphide electrodes at different cutoff voltages. Upon sodiation of Sn_4P_3 below 0.3 V a rapid amorphization process initially occurs and at 0.24 V a broad peak corresponding to Na_4Sn_4 appears at about 16°. This agrees with the findings Kim et al.[6] Similar behavior has also been observed for the lithiation of Sn_4P_3.[15] After further discharging the cell to 0.135 V, peaks from Sn_4P_3 could no longer be observed, while a new broad peak at about 35.8° corresponding to Na_5Sn_2 appeared. Figure 3b shows the XRD pattern measured at 0.005 V of fully sodiated Sn_4P_3 in detail. The pattern may be deconvoluted into contributions from Na_3P, Na_5Sn_2 and $Na_{15}Sn_4$. All of the above interpretations are in accordance with the voltage-phase data from Du et al.[11] and Baggetto et al.[10] However, the XRD patterns are broad and the peak assignments are not conclusive. It will be shown below that these peak assignments of the Na-Sn phases are in fact correct.

Mössbauer spectroscopy was used to analyze the phase coexistence during Sn_4P_3 in a more quantitative manner than possible by XRD. Room temperature ^{119}Sn Mössbauer effect spectra of Sn_4P_3 electrodes measured at different stages of sodiation are shown in Figures 4a–4e. The Sn_4P_3 crystal lattice contains two nonequivalent Sn sites, with a ratio of 1:1. Thus, the Mössbauer spectrum of Sn_4P_3 was fitted to two doublets, as shown in Figure 4a. The center shifts of the two doublets are 2.66 and 2.67, and the intensity ratio of the two doublets is 50.2:49.8. These are consistent with the 1:1 ratio of site occupancies. The center shift of the uncycled Sn_4P_3 is slightly smaller than the result reported by Häggström et al.[15] This slight difference may be caused by different synthesis methods of Sn_4P_3, as Häggström et al heated the sample under vacuum while high-energy ball milling was used here.

The Mössbauer spectrum collected from the sample at 0.3 V was fitted to three doublets in Figure 4b, one corresponding to the formation of $Na_{0.6}Sn$ and two corresponding to the two sites of Sn_4P_3. The fitting shows that the sample contains 88% Sn_4P_3 and 12% $Na_{0.6}Sn$, which means that only a small portion of Sn_4P_3 has reacted with Na at this voltage. This fitting agrees with the XRD pattern, where most of the Sn_4P_3 peaks remained unchanged at 0.3 V. The Mössbauer spectrum collected from the sample at 0.24 V was fitted to four doublets in Figure 4c, corresponding to $Na_{0.6}Sn$, Na_4Sn_4, and two sites of Sn_4P_3 respectively, with ratios of 18%, 62%, 10% and 10%. The Mössbauer spectrum collected from the sample at 0.135 V was fitted to two doublets in Figure 4d: Na_4Sn_4 and Na_5Sn_2, with ratios of 33% and 67%. The Mössbauer spectrum collected from the fully discharged sample

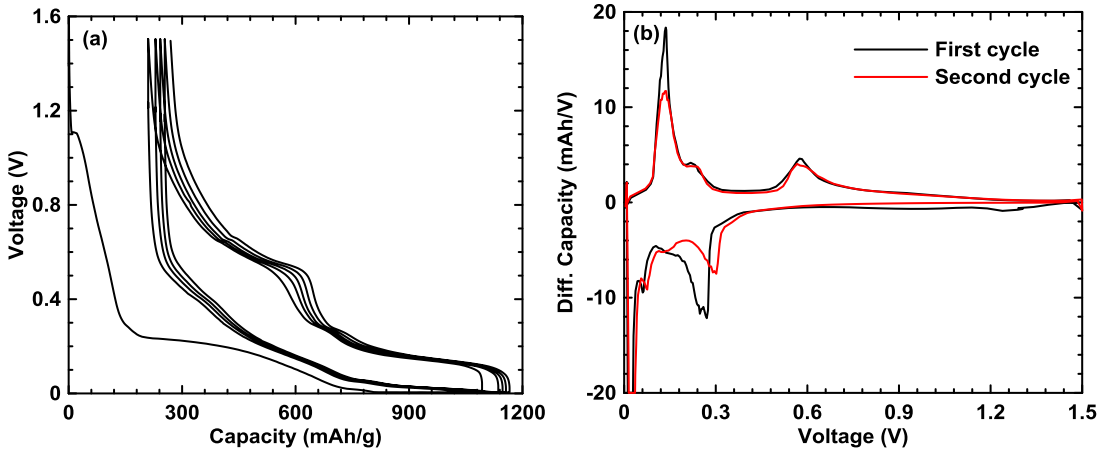

Figure 2. (a) Voltage curve of Sn_4P_3 electrode cycling with Na at a rate of C/20 (b) Differential capacity (dQ/dV) curve as a function of voltage for Sn_4P_3 during the first two cycles.

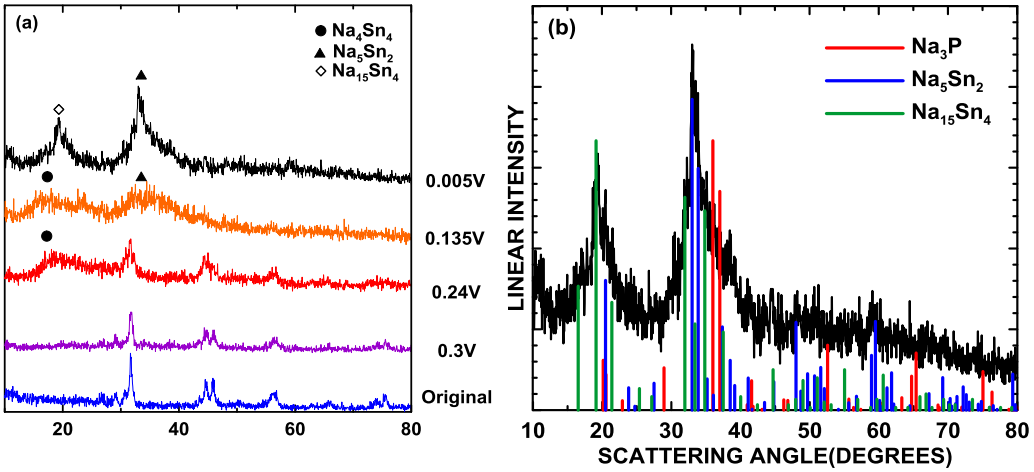

Figure 3. (a) Ex-situ XRD patterns of Sn_4P_3 electrodes at different cutoff voltages (b) ex-situ XRD pattern of the fully discharged Sn_4P_3 electrode.

in Figure 4e was fitted to two doublets, each representing Na_5Sn_2 and $Na_{15}Sn_4$ respectively. The ratios of the two compounds are 61% and 39%. In Figure 4e, the overall center shift of the fully discharged Sn_4P_3 (2.24 mm/s) is more positive compared with the fully sodiated pure tin (2.15 mm/s reported by Du et al.[11] and 2.18 mm/s reported by Baggetto et al.[10]). This indicates an incomplete sodiation of Sn_4P_3,

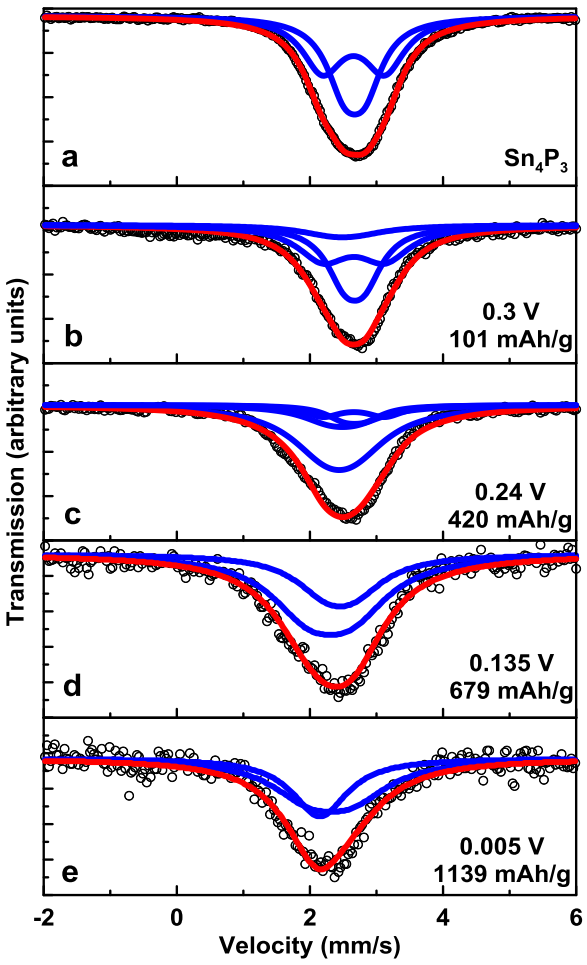

Figure 4. Ex-situ Mössbauer pattern collected at different cutoff voltages: (a) Original Sn_4P_3 (b) 0.3 V (c) 0.24 V (d) 0.135 V (e) 0.005 V. The inset shows the cutoff voltage on differential capacity curve pattern for each sample.

even though the cell was discharged to 0.005 V. This might have resulted from the low kinetics. For each sample, the capacity of each compound can be calculated from the area ratio obtained from the fits of the Mössbauer spectra. It is assumed that the formation of Na_3P and the solid electrolyte interphase (SEI) layer are responsible for rest of the capacity. Using this method the capacity distribution of the capacity can be calculated as a function of voltage. The area ratios of different phases and the capacity distribution of each sample are summarized in Table I. These results will be discussed in terms of the ex-situ observations below.

In Figure 5 the measured mean center shifts of the ex-situ Mössbauer spectra shown in Figure 4 are plotted as a function of the Na/Sn atomic ratio. For comparison, this ratio is also plotted for Na insertion into pure Sn, as reported by Du et al.[11] Both Sn and Sn_4P_3 show a trend of decreasing center shift with increasing sodiation. The Na-Sn system has a linear dependence of the center shift on the Na/Sn ratio. This decreasing center shift results from valence electrons being donated to the conduction band and additionally a reduction in

Table I. Relative area and capacity distribution derived from Mössbauer fitting result.

Materials	Relative Area	δ (mm/s)	Δ (mm/s)	Γ (mm/s)	Capacity (mAh/g)
Original Sn_4P_3		2.67			0
$Sn_4P_3^{site1}$	50%	2.67	0.32	0.32	0
$Sn_4P_3^{site2}$	50%	2.66	0.93	0.37	0
Sample at 0.3 V		2.66			101
$Sn_4P_3^{site1}$	44%	2.67	0.31	0.33	0
$Sn_4P_3^{site2}$	44%	2.66	0.93	0.46	0
$Na_{0.6}Sn$	12%	2.49	0.36	0.61	14
Na_3P+SEI					87
Sample at 0.24 V		2.51			420
$Sn_4P_3^{site1}$	10%	2.67	0.31	0.33	0
$Sn_4P_3^{site2}$	10%	2.66	0.93	0.32	0
$Na_{0.6}Sn$	18%	2.49	0.41	0.51	20
Na_4Sn_4	62%	2.45	0.43	0.64	119
Na_3P+SEI					281
Sample at 0.135 V		2.36			679
Na_4Sn_4	33%	2.45	0.42	0.57	62
Na_5Sn_2	67%	2.31	0.65	0.69	316
Na_3P+SEI					301
Sample at 0.005 V		2.24			1139
Na_5Sn_2	61%	2.31	0.65	0.69	288
$Na_{15}Sn_4$	39%	2.15	0	0.50	276
Na_3P+SEI					575

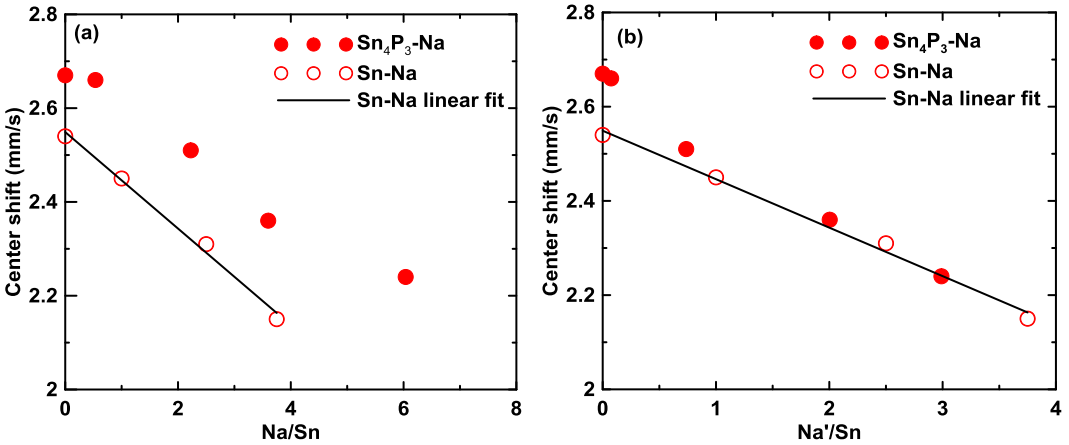

Figure 5. Center shifts plotted versus (a) the Na/Sn fraction or (b) the Na′/Sn fraction (as described in the manuscript) during sodiation of Sn_4P_3. Also shown in both graphs are the center shifts for the sodiation of pure Sn. A linear fit was added to the pure Sn data as a guide to the eye.

the number of Sn-Sn bonds as the Na content is increased.[11] In Figure 5a, the center shifts of Sn_4P_3 are always greater than those of Sn, for a given Na/Sn ratio. This is expected, since the sodium that reacts with any P during sodiation has no effect on Sn regions or their center shift. Therefore, when the same amount of sodium and active materials reacted, the magnitude of the deviations in the center shift in the Na–Sn_4P_3 system is always smaller than the Na–Sn system.

In order to correct for this effect, the measured mean center shifts are also plotted in Figure 5b as a function of the Na′/Sn atomic ratio, where the Na′ is the amount of sodium that has reacted with tin only, as derived from the Na-Sn alloy content measured by Mössbauer spectroscopy (listed in Table I). By this method the amount of Na reacting with P is not considered, and now the Sn_4P_3 center shifts are very close to those for Na-Sn alloys for high Na′/Sn contents (Na′/Sn $>$ 1). However, the center shifts of Sn_4P_3 are higher than those for Na-Sn alloys at low Na contents (Na′/Sn $<$ 1). This is because at the early stages of sodiation, unreacted Sn_4P_3 still exists in the electrode, and thus the overall center shift is more positive because of Sn-P interactions. As the sodiation progresses, Sn_4P_3 becomes consumed and is progressively replaced by Na-Sn phases and the center shift of the Sn_4P_3 electrode and Sn begin to converge. When Na′/Sn $\approx$ 1 all the Sn_4P_3 has reacted with Na and all the Sn is now in the form of Na-Sn phases. At higher Na contents the Sn_4P_3 and Sn electrode center shifts become identical.

By combining the results from electrochemical cells, XRD and Mössbauer spectroscopy, it can be concluded that as the sodium is inserted into Sn_4P_3, they most likely react according to the following equations:

$$Sn_4P_3 + Na \rightarrow Na_3P + Na_{0.6}Sn + Na_4Sn_4 \quad [1]$$

$$Na_{0.6}Sn + Na_4Sn_4 + Na \rightarrow Na_5Sn_2 + Na_{15}Sn_4 \quad [2]$$

It should be noted that neither Equations 1 or 2 are balanced and are only meant to show the reactants and products. Here Na first reacts with Sn_4P_3 to form Na_3P, $Na_{0.6}Sn$, and then Na_4Sn_4, according to Equation 1. After this, the Na-Sn phases react with Na to make Na_5Sn_2 and $Na_{15}Sn_4$, according to Equation 2. A similar process was also suggested by Pérez-Vicente et al.,[25] when Sn_4P_3 reacted with Li in a electrochemical cell: the lithiation of Sn starts almost immediately upon lithiation, and then then the lithiation of Sn and P take place simultaneously.

Conclusions

Sn_4P_3 was prepared using high-energy ball milling, and Sn_4P_3 composite electrodes were cycled with Na in half cells. These electrodes were collected at different cutoff voltages and were studied by ex-situ X-ray diffraction and Mössbauer effect spectroscopy. The results suggest that upon sodiation, Sn and P begin to react with sodium simultaneously, resulting in the formation of $Na_{0.6}Sn$, and Na_4Sn_4, phases. To account for the additional capacity observed, Na_3P is likely initially formed simultaneously with the $Na_{0.6}Sn$ phase. After further sodiation, the Na-Sn phases react with more sodium and eventually form $Na_{15}Sn_4$. These findings are consistent with the behavior of Sn_4P_3 in Li cells. This provides a good example of how Mössbauer spectroscopy can provide insight into the mechanism of metal alloying reactions in metal ion cells.

Acknowledgments

The authors acknowledge funding from NSERC and 3M Canada Co. under the auspices of the Industrial Research Chair and Discovery grant programs. We also acknowledge the support of other partners that fund the Facilities for Materials Characterization managed by the Institute for Research in Materials.

References

1. N. Yabuuchi, K. Kubota, M. Dahbi, and S. Komaba, *Chem. Rev.*, **114**, 11636 (2014).
2. M. Jäckle, A. Groß, M. Jäckle, and A. Groß, *J. Chem. Phys.*, **141**, 174710 (2014).
3. T. T. Tran and M. N. Obrovac, *J. Electrochem. Soc.*, **158**, A1411 (2011).
4. M. N. Obrovac and V. L. Chevrier, *Chem. Rev.*, **114**, 11444 (2014).
5. J. Qian, Y. Xiong, Y. Cao, X. Ai, and H. Yang, *Nano Lett.*, **14**, 1865 (2014).
6. Y. Kim et al., *Adv. Mater.*, **26**, 4139 (2014).
7. J. S. Thorne, J. R. Dahn, M. N. Obrovac, and R. A. Dunlap, *J. Power Sources*, **216**, 139 (2012).
8. R. A. Dunlap, O. Mao, and J. R. Dahn, *Phys. Rev. B*, **59**, 3494 (1999).
9. B. León, J. I. Corredor, J. L. Tirado, and C. Pérez-Vicente, *J. Electrochem. Soc.*, **153**, A1829 (2006).
10. L. Baggetto et al., *J. Mater. Chem. A*, **2**, 18959 (2014).
11. Z. Du, R. A. Dunlap, and M. N. Obrovac, *J. Alloys Compd.*, **617**, 271 (2014).
12. R. Fielden and M. N. Obrovac, *J. Electrochem. Soc.*, **162**, A453 (2015).
13. B. N. Wilkes, Z. L. Brown, L. J. Krause, M. Triemert, and M. N. Obrovac, *J. Electrochem. Soc.*, **163**, A364 (2016).
14. Y.-U. Kim, C. K. Lee, H.-J. Sohn, and T. Kang, *J. Electrochem. Soc.*, **151**, A933 (2004).
15. L. Häggström, J. Gullman, T. Ericsson, and R. Wäppling, *J. Solid State Chem.*, **13**, 204 (1975).